Multi-transformations in rapid solidification of highly undercooled hypoeutectic Ni–Ni_3B alloy melt

Junfeng Xu
The Shaanxi Key Laboratory of Photoelectric Functional Materials and Devices, Xi'an Technological University, Xi'an, Shaanxi Province 710021, People's Republic of China

Di Zhang
State Key Laboratory of Solidification Processing, Northwestern Polytechnical University, Xi'an, Shaanxi Province 710072, People's Republic of China

Feng Liu[a)]
The Shaanxi Key Laboratory of Photoelectric Functional Materials and Devices, Xi'an Technological University, Xi'an 710021, People's Republic of China; and State Key Laboratory of Solidification Processing, Northwestern Polytechnical University, Xi'an, Shaanxi Province 710072, People's Republic of China

Zengyun Jian
The Shaanxi Key Laboratory of Photoelectric Functional Materials and Devices, Xi'an Technological University, Xi'an, Shaanxi Province 710021, People's Republic of China

(Received 19 June 2015; accepted 9 September 2015)

The solidification of undercooled Ni–3.3 wt% B alloy was studied by high-speed video analysis and microstructural analysis. For moderate initial undercooling (ΔT_p = 75 K), the solidification interface for primary phase transformation manifests a shape of a planar dendrite, and possesses an constant growth velocity, for eutectic transformation whereas the interface presents multi-dendrite shape and spasmodic growth, so that a constant velocity cannot describe the interface exactly. These differences suggest that primary phase solidification is controlled by far-distance diffusion while eutectic solidification by short-distance diffusion. For large initial undercooling (ΔT_p = 262 K), a kinds of large "white dendrites", which is in fact composed of multiple phases, were found in the microstructure, from inside to outside of which, the eutectic phase changes from dot phases (anomalous structure) to irregular eutectic and then to regular eutectic, indicating that the center of "white dendrites" may be the nucleation zone of eutectic reaction.

I. INTRODUCTION

Recently, researchers have made many studies on solidification of undercooled melts.[1–8] However, most of these studies focus on the solidification possessing single-transformation, such as that of single phase alloy or eutectic alloy[1–8] with single transformation. Based on the single transformation, the classical theories mainly concentrate on the growth velocity of single dendrite phase, such as Boettinger–Coriell–Trivedi model,[9] or eutectic phase, such as Trivedi–Magnin–Kurz[10] and Li–Zhou models.[11] Generally, for most commercial alloys, the compositions are always not located in eutectic point, i.e., off-eutectic alloy, so that it is out of the classical theory. With this consideration, the theories were developed continuously, for instance, the famous couple zone theory[12] derived for off-eutectic alloy. Couple zone theory can be used to decide the competitive growth of eutectic and dendrites for off-eutectic alloys. Nevertheless, this theory was based on directional solidification[13] and still has not taken the multi-transformations into account, thus it cannot describe the eutectic transformation after primary dendrite for off-eutectic alloy. Even though some researchers applied this theory to the undercooled solidification of off-eutectic alloy, it is only for the composition near eutectic where only primary dendrites or eutectic transformation occurs. So far, the reports about the undercooled solidification of off-eutectic alloy only received limited investigations. As a typical eutectic alloy, Ni–B alloy has some interesting applications such as nanocrystalline or amorphous films, electroless coatings, brazing filler metals, and master alloys.[14–16] More importantly, the undercooled melt of this alloy has obvious multi-transformation process during solidification.[17,18] Accordingly, hypoeutectic Ni–3.3 wt% B alloy are chosen to study the undercooled solidification of off-eutectic alloy.

In the previous work, the solidification interfaces and cooling curves associated with the rapid solidification behavior of Ni–B alloy had been revealed.[17,18] However, the details for each transformation have not been analyzed, and the character of the microstructure solidified

Contributing Editor: Yang-T. Cheng
[a)]Address all correspondence to this author.
e-mail: liufeng@wpu.edu.cn
DOI: 10.1557/jmr.2015.295

 © Materials Research Society 2015

https://doi.org/10.1557/jmr.2015.295 Published online by Cambridge University Press

from large initial undercooling has not been shown completely. In the present work, the true consequence of rapid solidification of hypoeutectic Ni–3.3 wt% B alloy will be displayed detailed by High-speed video (HSV) and highly sensitive infrared thermometer techniques. The transformations of primary dendrite and eutectic phases from moderate undercooling are mainly discussed. And then the microstructures solidified from large undercooling will be analyzed by optical microscope and scanning electron microscope (SEM). The objective is to further explore rapid solidification behavior of off-eutectic alloy, which can be quite helpful for multi-transformation theory study.

II. EXPERIMENTAL

The Ni–3.3 wt% B eutectic alloy samples weighed about 4 g, each of which was prepared by melting 99.9% Ni blocks and 99% B powders. To protect the alloy from oxidization and achieve high undercooling, the glass fluxing technique was adopted. B_2O_3 glass was used which is made from the analytical reagents that melted in a fused silica crucible, and then slowly heated and kept under a molten state at temperature of 1073 K for 6 h aimed to be fully homogenized and dehydrated. It could remove impurities from the melt as denucleating agents. During experiment the sample was placed into a quartz–glass crucible, together with some pieces of B_2O_3 glass. The crucible was positioned at the middle of the high frequency induction coil and located in a vacuum chamber. After the vacuum chamber evacuated to 1×10^{-6} mbar and backfilled to 600 mbar with high purity Ar gas, the sample was heated until fully melt, keep the melt at a temperature higher 100–200 K than the melting point for several minutes, and then turn off the power to make the sample solidifies. To obtain different undercoolings, this process was repeated cyclically. Thermal history of the alloy was monitored by a monocolor highly sensitive pyrometer, the relative accuracy and response time of which are 10 K and 2 ms, respectively. A HSV instrumentation system was used to in situ observe the solidification behavior. The camera system developed by Olympus is capable of operation at rates up to 150,000 frames per second, meanwhile the resolution of ratio could reach 1280 × 1024. To record the liquid/solid interface clearly, the aperture always is minimized. For microstructure observation, a solution consisting of 5 g $FeCl_3$, 10 mL HCl, and 50 mL H_2O was used to etch the as-solidified specimens.

III. RESULTS

A. Cooling curves

The cooling curves of Ni–3.3 wt% B alloy with different undercoolings are shown in Fig. 1. The undercooling for primary solidification is defined as $\Delta T_p = T_L - T_n$, where T_L is the melting point (about 1450 K) and T_n is the initial nucleation point. The undercooling for eutectic solidification is defined as $\Delta T_e = T_e - T_{en}$, where T_e is the equilibrium eutectic temperature (about 1366 K here) and T_{en} the starting temperature for eutectic transformation. If there are three recalescences in the cooling curve, besides ΔT_p and ΔT_e, there exists a undercooling ΔT_r ($=T_e - T_r$) for the third transformation, where T_r is the start-temperature for this transformation. It is obvious that the cooling curves as well as the microstructures for samples 1 and 2 are much different, so as to the microstructures, suggesting that the cooling curves and the microstructures may have some corresponding relationships.

As can be seen from Fig. 1, there are two recalescences during solidification of sample 1. The primary solidification and the eutectic solidification are initiated at $\Delta T_p \sim 75$ K ($=1450$ K $- 1375$ K) and $\Delta T_e \sim 64$ K ($=1366$ K $- 1302$ K), respectively. In view of the two recalescences of sample 1, the solidification is according to the equilibrium phase diagram.

The cooling curve of sample 2 (Fig. 1) shows that the melt of Ni–3.3 wt% B alloy undergoes three recalescences during its solidification when the initial undercooling is $\Delta T_p \sim 262$ K. The second undercooling is measured as $\Delta T_e \sim 143$ K. Whereas, the second transformation just achieves a maximal recalescence temperature (MRT) of ~1250 K, indicating that the metastable eutectic reaction occurs. Then after a short isothermal solidification, the third recalescence peak appears in the cooling curve with $\Delta T_r = 135$ K.

B. Microstructures

Figures 2 and 3 show the optical microstructures of the cross sections of samples 1 and 2, respectively. The different colors of the phases are due to the diversified corrosion resistance of each phase. The present corrosive (Fe_3Cl, HCl) can mainly etch the α-Ni phase but not Ni_3B

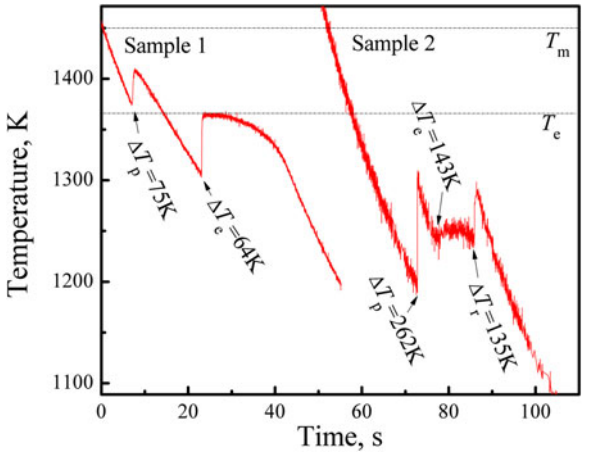


FIG. 1. Cooling curves of sample 1 and sample 2, respectively.

https://doi.org/10.1557/jmr.2015.295 Published online by Cambridge University Press

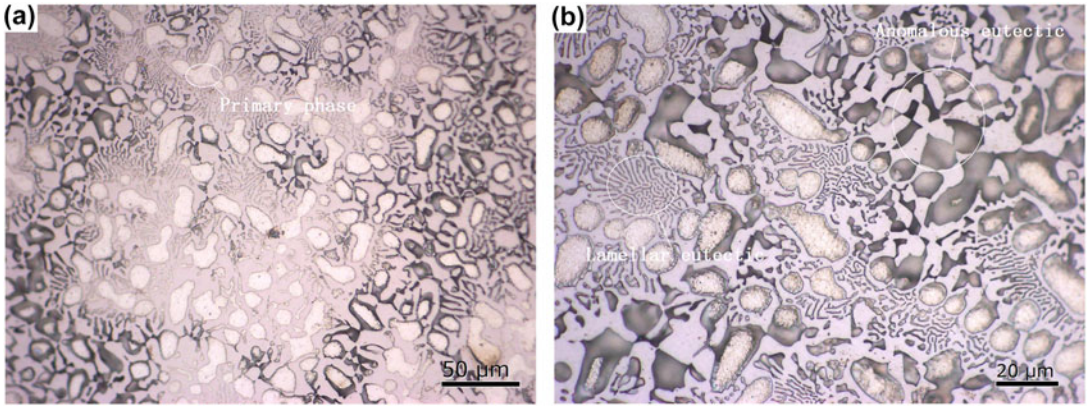


FIG. 2. As-solidified microstructure of sample 1($\Delta T_p \sim 75$ K and $\Delta T_e \sim 64$ K): (a) low-magnification optical micrograph; (b) high-magnification optical micrograph.

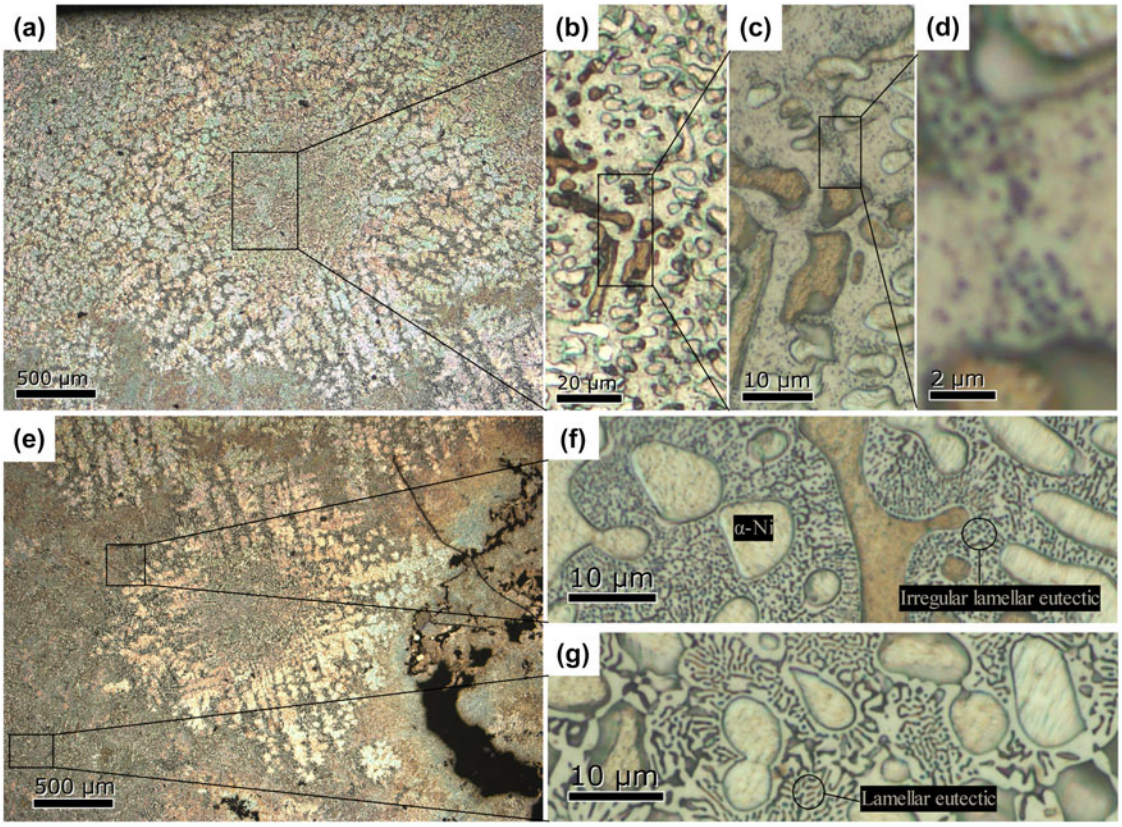


FIG. 3. As-solidified microstructure of sample 2 ($\Delta T_p \sim 262$ K, $\Delta T_e \sim 143$ K and $\Delta T_r = 135$ K): (a) and (e) low-magnification optical micrograph; (b), (c), (d), (f) and (g) high-magnification optical micrograph.

phase, so that the two phases can be intuitively separated. Since different crystallographic orientations of α-Ni phase have different corrosion resistance, some α-Ni phase shows dark color while some other shows light one.

The low-magnification optical micrograph of sample 1 [Fig. 2(a)] shows that it consists of primary dendrite phase (α-Ni), lamellar eutectic, and anomalous eutectic (Ni–Ni_3B). The lateral dimension of the dendrite is about 10 μm. The lamellar eutectic mainly distributes in the interdendritic regions and the lamellar spacing is about 2.2 μm measured through high-magnification micrograph [Fig. 2(b)].

For the optical microstructure of sample 2, it can be seen that in the low-magnification micrograph [as shown in Figs. 3(a) and 3(e)], the microstructure consists of several developed "white dendrite" and dark matrix. However, it is totally different in its high-magnification micrograph. As shown in Figs. 3(b)–3(d), the center of

https://doi.org/10.1557/jmr.2015.295 Published online by Cambridge University Press

the "white dendrite" consists of primary phase (α-Ni), dot phases (Ni), and bright matrix. The primary phase apparently appears as granular shape with a lateral dimension of 4 μm, which is smaller than that of sample 1 (Fig. 2). As for the dot phases, they are distributed nonuniformly in the matrix. Figures 3(f) and 3(g) show the structures outside of the "white dendrite". Compared with the structures in the center, the morphologies of primary phase (α-Ni) and the bright matrix (Ni_3B) are not changed, but the irregular lamellar eutectic (near the "white dendrite") and regular lamellar eutectic (far from the "white dendrite") can be observed. That is, from the inside to the outside of the "white dendrite", the eutectic phase changes from dot phases to irregular eutectic and then to regular eutectic. It can be inferred that: (i) the formation of the large "white dendrite" has no influence on the primary solidification so that the size of primary α-Ni phase remains invariable; (ii) the formation of the dot phases or eutectic phases depends on the growth of "white dendrite", which changes the composition distribution of residual liquid for the third transformation. So the "white dendrite" forms after the primary phase transformation but before the last stable eutectic transformation.

Besides, there are two kinds of dot phases, one is sparsely distributed in the matrix [Ni_3B, see Fig. 3(c)], and the other is clustered together in the boundary of matrix phase shown as network boundary [Fig. 3(d)]. The former may be from precipitation of metastable matrix, while the latter is from solidification (i.e., the third transformation). In addition, SEM analysis can evidence that the network boundary is shrinkage anomalous eutectic (Fig. 4).

To further observe the structure, SEM images of sample 2 are shown in Fig. 4. In the low-magnification image, a "white dendrites" and "dark matrix" can be found [Fig. 4(a)]. Since the α-Ni structures, including the α-Ni granule and eutectic α-Ni, are easily etched, the remaining skeleton is Ni_3B phase. From the high magnification images of the center of the "white dendrite" in Figs. 4(c), 4(e), 4(g), and 4(h), we can identify that the structure consists of primary phase (α-Ni), dot phases (Ni), and bright matrix. Therein, the dot phases are so small that it may be precipitation from the matrix.

From the high magnification image of the outside of "white dendrites" in Figs. 4(b), 4(d), and 4(f), we can find many Ni_3B grains and some dark holes. The dark holes are the trace of α-Ni phase. The alternative distribution of Ni and Ni_3B phases indicates that the phase outside the "white dendrite" is anomalous eutectic. Moreover, connectivity of the dark region indicates that the primary α-Ni and eutectic Ni are cohesive [see Figs. 4(d) and 4(f)].

C. Solidification interface

To further study dendrite growth kinetics, the HSV images for the solidification process of Ni–3.3 wt% B alloy at different undercoolings are shown in Fig. 5, where the dark regions are the undercooled melt, while the bright ones are the growing solid. For sample 1, there are two transformations, corresponding to the two recalescences in the cooling curves (Fig. 1). For the first transformation [L → α-Ni, as shown in Fig. 5(a)], a small bright point initially appears at the center of sample, and then spreads throughout the sample manifesting a shape of a planar dendrite. For the second transformation [L → Ni/Ni_3B, as shown in Fig. 5(b)], the morphology of solidification front is shaped as multi-small-dendrite spreads throughout the sample space [Fig. 5(b)].

For sample 2, since the second undercooling is very small and the solidification interface is not clear, only the first and the third transformations were recorded as shown in Figs. 5(c) and 5(d), respectively. For the first transformation, the morphology of solidification front shown a spherical shape with a small serration front spreads radically throughout the sample, which indicates that the solidification interface for the primary transformation changes from large dendritic to spherical shapes with the increase of undercooling. For the third transformation, the morphology of the interface shows as a similar spherical front throughout the sample. For the second transformation, only at a rather larger undercooling, the solidification interface can be observed, manifesting as some cluster-like shapes,[17] which are very similar to the shape of the "white dendrite".

To study the growth velocity, Fig. 6 shows the moving distance (D) of solidification interface as a function of time (t) for every transformation. It can be found that an approximate linear relation exists between the moving distance and time, implying a nearly constant interface velocity as evaluated by the slope of the fitting line. For sample 1, the relationships between moving distance and time for primary and eutectic solidifications can be fitted by $D = 23.21t + 0.1831$ and $D = 85.68t - 0.4281$, respectively. Therefore, the average velocities for transformations of L → α-Ni and L → Ni + Ni_3B are derived as 23.21 and 85.68 mm/s, respectively. Analogously, for sample 2, the relationships for the first transformation (primary solidification) and the third transformation (stable eutectic solidification) can be fitted by $D = 141.5t - 0.0048$ and $D = 126.6t + 0.0179$, as a result, the growth velocities for L → α-Ni and L → Ni + Ni_3B are determined as 141.5 and 126.6 mm/s, respectively. Based on the above analysis, the growth velocity of primary phase increases with increasing ΔT_p.

IV. DISCUSSIONS

In the preceding sections, the cooling curves, microstructures and morphologies of solidification interfaces of samples 1 and 2, have been demonstrated, which shows that relating the microstructures and the cooling curves may be possible. In an attempt to explore this relation, it

https://doi.org/10.1557/jmr.2015.295 Published online by Cambridge University Press

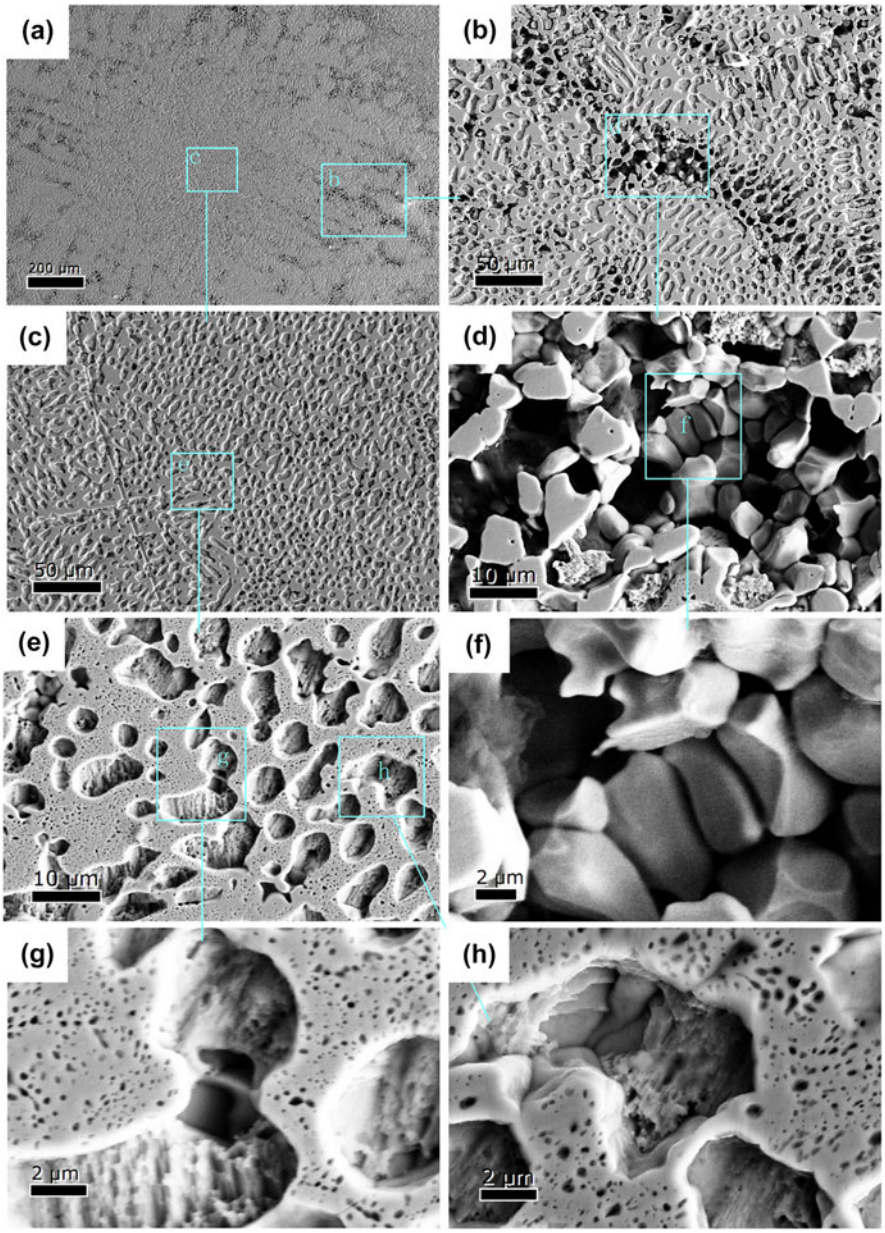


FIG. 4. SEM images of sample 2 with $\Delta T_p \sim 262$ K, $\Delta T_e \sim 143$ K and $\Delta T_r = 135$ K: (a) low-magnification micrograph of the "white dendrite"; (b), (d) and (f) high magnification image of the outside of "white dendrite"; (c), (e), (g) and (h) high magnification image of the inside of "white dendrite".

is necessary to discuss the influence of the undercoolings on the solidification pathways, microstructures, growth velocities, and the morphologies of solidification front.

A. Solidification pathways

According to sample 1, the first recalescence corresponds to the nucleation and growth of the primary dendrite phase (L → α-Ni), and then dendrite partially breaks due to the release of latent heat [Fig. 2(a)]. Subsequently, Ni_3B phase nucleates and grows during the second recalescence, which activates the eutectic reaction, L → Ni + Ni_3B. Thus at the peak of the second recalescence, the anomalous eutectic forms. When the system temperature reaches about equilibrium eutectic melting point (1366 K), the residual liquid totally transforms to regular eutectic (Ni/Ni_3B). Accordingly, the final microstructure of sample 1 consists of the primary phase α-Ni, anomalous eutectic and lamellar eutectic phases [Figs. 2(a) and 2(b)].

Analogously, the first recalescence of sample 2 corresponds to nucleation and growth of primary phase α-Ni, i.e., L → α-Ni. As compared with sample 1, the fragments of dendrite for sample 2 becomes more serious as

https://doi.org/10.1557/jmr.2015.295 Published online by Cambridge University Press

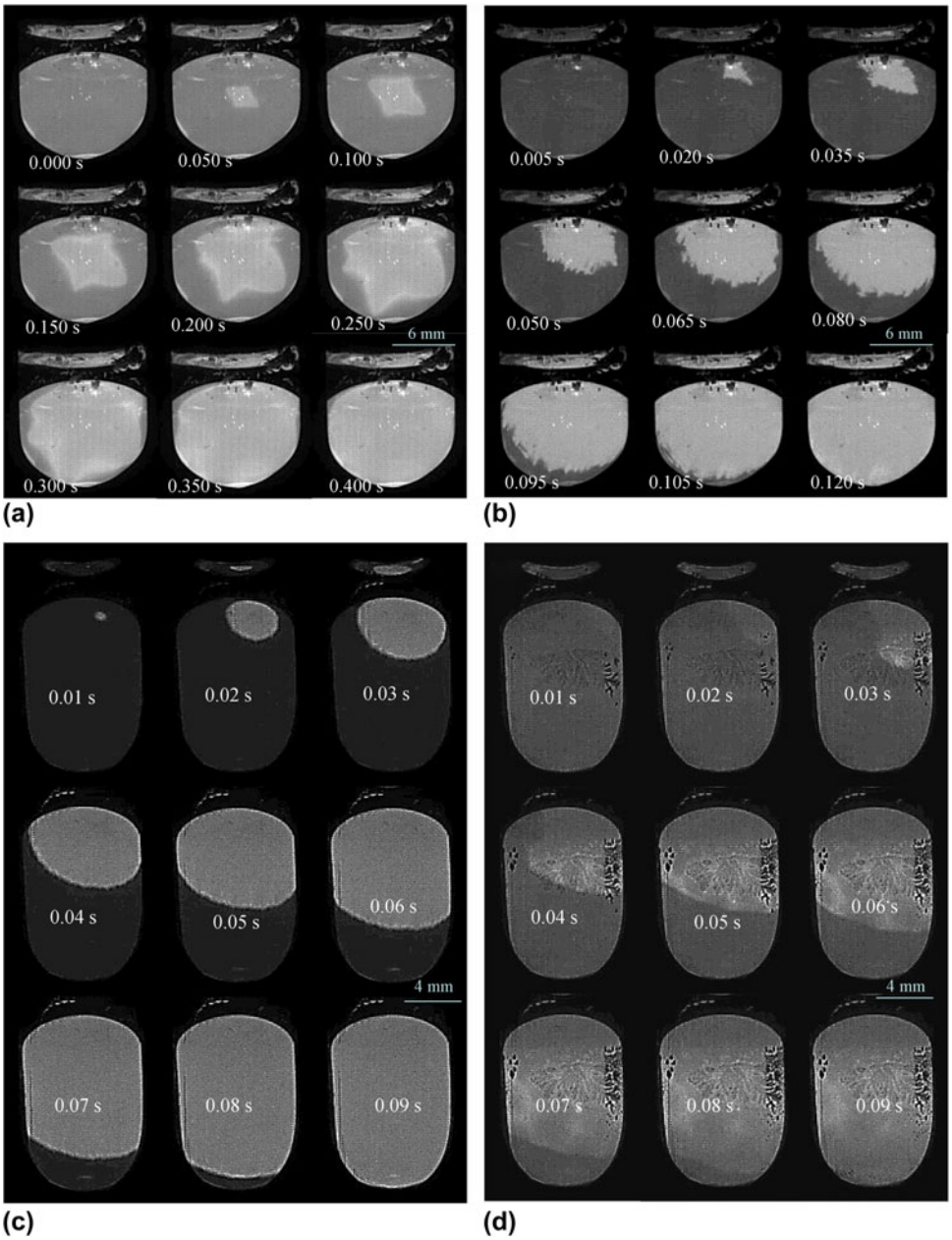


FIG. 5. Recalescence behaviors of samples 1 and 2, as captured by HSV: (a) primary solidification of sample 1; (b) eutectic solidification of sample 1; (c) primary solidification of sample 2; (d) stable eutectic solidification (corresponding to the third recalescence) of sample 2.

a result of latent heat release induced by the larger undercooling, and meanwhile the primary α-Ni in the final structure presents as granular shape (see Fig. 3). Then in the second recalescence, the metastable eutectic reaction ($L \rightarrow Ni_{23}B_6 + Ni$) occurs, as demonstrated elsewhere,[17,18] leading to an isothermal plateau appearing in the cooling curve (it is considered as eutectic reaction because the eutectic reaction always shows an isothermal plateau in the cooling curve). Since $Ni_{23}B_6$ phase is thermodynamically unstable, it decomposes into $Ni_3B + Ni$ with Ni_3B as the matrix and Ni as the dot phase at a certain time after the second recalescence. As soon as Ni_3B appears, the stable eutectic reaction ($L \rightarrow Ni + Ni_3B$) is activated, and then the third recalescence process arises, which gives rise to the anomalous eutectic (Ni/Ni_3B). It is worth noting that MRT of the third reaction is above 1250 K (i.e., metastable eutectic point) but below 1366 K (i.e., stable eutectic point), which confirms that the reaction is eutectic transformation from residual liquid. Since the residual liquid after two

https://doi.org/10.1557/jmr.2015.295 Published online by Cambridge University Press

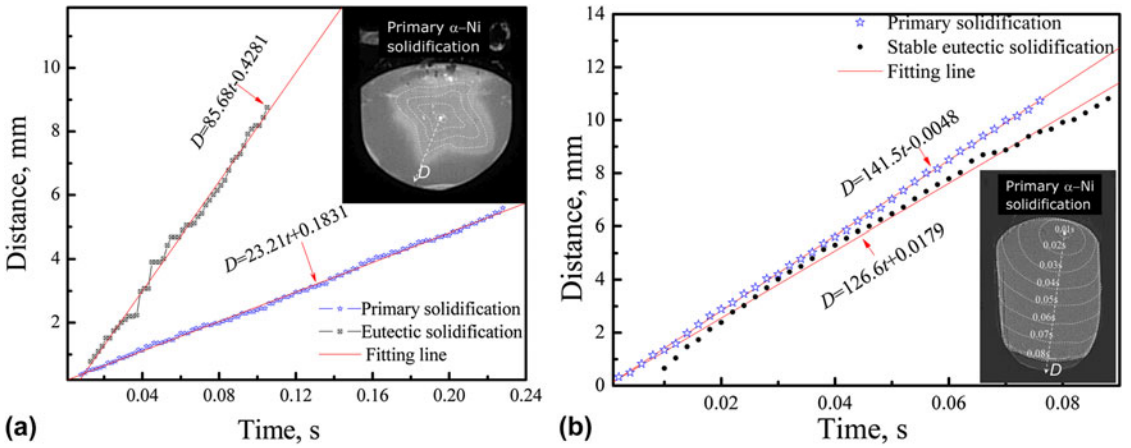


FIG. 6. Moving distance (D) of the solidification interface as a function of time (t): (a) Sample 1; (b) Sample 2.

transformations is little, the obtained anomalous eutectic shrinks as a network boundary [see Figs. 4(b) and 4(d)].

From Sec. 3.2, the "white dendrite" forms after the primary α-Ni formation, but before the last eutectic reaction, hence it is recognized as the trace of metastable eutectic reaction (L → $Ni_{23}B_6$ + Ni). However, metastable eutectic deduction is hard to interpret the outwardly dendritic structure, unless that $Ni_{23}B_6$ is the prevenient phase and grows first for metastable eutectic ($Ni_{23}B_6$/Ni), then the other phase(Ni) grows following, thus, the profile of this eutectic shows as a large $Ni_{23}B_6$ dendrite. Another possible for the "white dendrite" appearance is that in the second recalescence the metastable phase transformation L → $Ni_{23}B_6$ occurs, and $Ni_{23}B_6$ grows as dendrite shapes due to the smaller undercooling [=1250 K − (1366 K − ΔT_e) = 27 K] and longer growth time (the isothermal plateau in the cooling curve, see Fig. 1). In subsequence, Ni_3B nucleation and the third transformation, L → Ni + Ni_3B, is activated, which results the eutectic structure around the "white dendrite", meanwhile the "white dendrite" subsequent decomposes into the matrix and the very fine dispersion of submicrometer dark dot [Fig. 3(d)]. This assumption can interpret the origin of "white dendrite" well, but it is hard to understand why the single metastable phase ($Ni_{23}B_6$) can solidify from liquid after primary solidification. Generally the occurrence of eutectic transformation after primary solidification is understandable, so this question waits for continuing to study.

The second transformation (L → Ni + $Ni_{23}B_6$ or L → $Ni_{23}B_6$) has an effect on the solution distribution of the residual liquid as well as the third transformation (the stable eutectic reaction, L → Ni + Ni_3B). The work of Mullis et al. revealed that, for eutectic transformation, from the nucleation zone to outside zone, the eutectic changes from anomalous structure to lamellar structure.[19] For the present study [Fig. 4], it can be found that the morphology of eutectic changes from dot phase or anomalous structure (inside the "white dendrite") to lamellar structure (outside the "white dendrite"), which indicates that the center of the "white dendrite" is also the nucleation zone of the eutectic reaction.

B. Velocity and morphology of solidification front

Our previous study shows that the solidification behaviors mainly depend on the undercooling of eutectic transformation (ΔT_e) and there is a critical undercooling ΔT_e^* ~ 140 K for the alloy investigated here. If $\Delta T_e < \Delta T_e^*$, there are two recalescences (primary solidification + eutectic transformation) in the cooling curves.[18] In this case, the multi-dendrite solidification front changes more pronounced with increasing ΔT_e. If $\Delta T_e > \Delta T_e^*$, there are three recalescences (primary phase + metastable eutectic + stable eutectic transformations).[18]

For sample 1, although the undercooling of primary solidification (75 K) is larger than that of eutectic solidification (64 K), the growth velocities of primary phase (23.21 mm/s) is much smaller than that of eutectic phase [85.68 mm/s, Fig. 6(a)]. For sample 2, the undercooling of primary solidification (262 K) is far larger than that of stable eutectic solidification (135 K), and the growth velocity of primary phase (141.5 mm/s) is closed to that of eutectic phase [126.6 mm/s, Fig. 6(b)]. This indicates that under same undercooling, the driving force for eutectic growth is larger than that for primary solidification. In the other words, the resistance of eutectic growth is smaller than that of primary solidification, and thus the growth of eutectic is faster than that of primary phase. This is mainly attributed to the short- or long-distance diffusion of solute atoms in front of solidification interface. The growth of primary dendritic phase is controlled by long-distance diffusion of Ni atoms far from interface, but the eutectic growth is controlled by short-distance diffusion since the solute

https://doi.org/10.1557/jmr.2015.295 Published online by Cambridge University Press

atoms for growth come from the interface front of the adjacent eutectic phase.

In addition, from the two transitions of sample 1, we can find that the interface front for primary solidification [Fig. 5(a)] is more smooth and stable than that for eutectic solidification [Fig. 5(b)]. The whole shape of the primary solidification looks like a dendrite and the average velocity of the solidification interface can be approximated as a constant from Fig. 6(a). Whereas, the process of the solidification front for eutectic solidification is spasmodic (a series of jumps and pauses) in that the interface is instable [Fig. 6(a)]. The local relationship of the distance versus time is not linear. It may be also attributed to the short-distance diffusion for eutectic solidification where Ni and Ni_3B phases grow alternately, and the solid–liquid interface consists of a series of start–stop jumps. Similar phenomenon has already been found in Ag–Cu eutectic alloy by Clopet et al.[6] In addition, it also suggests that a constant interface velocity of eutectic solidification may not reflect the actual process for a certain undercooling. In present no model of eutectic growth can explain the observed growth mode.

V. CONCLUSIONS

The undercooled solidification of Ni–3.3 wt% B alloy was studied by in situ imaging of the solidification front using HSV analysis and microstructural analysis of the as-solidified samples. If ΔT_p = 75 K, the transformations of primary solidification and eutectic transformation occur; if ΔT_p = 262 K, primary transformation, metastable eutectic transformation, and stable eutectic transformation occur during solidification, resulting in the microstructure of primary phase + dot phases + matrix + network boundary, where the network boundary is evidenced to be a shrinkage anomalous eutectic by SEM analysis.

For primary solidification (ΔT_p = 75 K), the morphology of solidification front presents as a smooth dendritic tip and the interface velocity can be approximated as a constant, V = 23.21 mm/s. For eutectic solidification (ΔT_e = 64 K), the solidification front displays as multi-dendrite shape and spasmodic growth, thus a constant velocity cannot describe the interface exactly. The characteristics of interface morphologies suggest that the primary transformation is controlled by far-distance diffusion while the eutectic transformation is controlled by short-distance diffusion. In addition, "white dendrite", was observed in the sample with large initial undercooling (ΔT_p = 262 K). From the inside to the outside of the "white dendrite", the eutectic phase changes from dot phase (anomalous structure) to irregular eutectic and then to regular eutectic, which indicates the center of "white dendrite" is the nucleation zone of eutectic, and it also confirms the origin of anomalous eutectic proposed by Mullis.[19]

ACKNOWLEDGMENTS

The authors are grateful for the National Basic Research Program of China (Nos. 2013CB632904 and 2011CB610403), the Natural Science Foundation of China (Nos. 51171136, 51301125, 51401156, and 51371133), the Natural Science Basic Research Plan in Shaanxi Province of China (No. 2014JM6225), the Fund of Shaanxi Province Thin Film Technology and Optical Test Open Key Laboratory (No. ZSKJ201403) and the President fund of Xi'an Technological University (No. XAGDXJJ1307). J.F. Xu expresses thanks to S.J. Song, M.M. Gong, X.L. Xu, and S. B. Li for their help in this work.

REFERENCES

1. K. Kuribayashi, H. Kato, K. Nagayama, Y. Inatomi, and M.S. Vijaya Kumar: An experimental verification of a criterion for forming metastable phases in containerless solidification. *J. Appl. Phys.* **117**, 154905 (2015).
2. E.G. Castle, A.M. Mullis, and R.F. Cochrane: Evidence for an extended transition in growth orientation and novel dendritic seaweed structures in undercooled Cu–8.9 wt%Ni. *J. Alloys Compd.* **615**, 612 (2014).
3. E.G. Castle, A.M. Mullis, and R.F. Cochrane: Mechanism selection for spontaneous grain refinement in undercooled metallic melts. *Acta Mater.* **77**, 76 (2014).
4. D.M. Herlach: Non-equilibrium solidification of undercooled metallic melts. *Mater. Sci. Eng., R* **12**, 177 (1994).
5. C.R. Clopet, R.F. Cochrane, and A.M. Mullis: The origin of anomalous eutectic structures in undercooled Ag–Cu alloy. *Acta Mater.* **61**, 6894 (2013).
6. C.R. Clopet, R.F. Cochrane, and A.M. Mullis: Spasmodic growth during the rapid solidification of undercooled Ag–Cu eutectic melts. *Appl. Phys. Lett.* **102**, 031906 (2013).
7. L. Liu, J.F. Li, and Y.H. Zhou: Solidification interface morphology pattern in the undercooled Co–24.0 at.% Sn eutectic melt. *Acta Mater.* **59**, 5558 (2011).
8. J.F. Li, W.Q. Jie, S. Zhao, and Y.H. Zhou: Structural evidence for the transition from coupled to decoupled growth in the solidification of undercooled Ni–Sn eutectic melt. *Metall. Mater. Trans. A* **38**, 1806 (2007).
9. W.J. Boettinger, S.R. Coriell, and R. Trivedi: Application of dendritic growth theory to the interpretation of rapid solidification microstructures. In *Rapid Solidification Processing: Principles and Technologies IV*; R. Mehrabian and P. A. Parrish, eds. (Baton Rouge, LA: Claitor's Publishing Division, 1988), p. 13.
10. R. Trivedi, P. Magnin, and W. Kurz: Theory of eutectic growth under rapid solidification conditions. *Acta Metall.* **35**, 971 (1987).
11. J.F. Li and Y.H. Zhou: Eutectic growth in bulk undercooled melts. *Acta Mater.* **53**, 2351 (2005).
12. W. Kurz and D.J. Fisher: Dendrite growth in eutectic alloys: The coupled zone. *Int. Mater. Rev.* **24**, 177 (1979).
13. M. Trepczyńska-Łent: Competitive growth and couplet growth zone in eutectic alloys in directional solidification. *J. Pol. CIMAC* **5**, 229 (2010).
14. K.H. Lee, D. Chang, and S.C. Kwon: Properties of electrodeposited nanocrystalline Ni–B alloy films. *Electrochim. Acta* **50**, 4538 (2005).

https://doi.org/10.1557/jmr.2015.295 Published online by Cambridge University Press

15. K. Krishnaveni, T.S.N. Sankara Narayanan, and S.K. Seshadri: Electrodeposited Ni–B coatings: Formation and evaluation of hardness and wear resistance. *Mater. Chem. Phys.* **99**, 300 (2006).
16. Y. Guo, X. Liu, M.U. Azmat, W. Xu, J. Ren, Y. Wang, and G. Lu: Hydrogen production by aqueous-phase reforming of glycerol over Ni–B catalysts. *Int. J. Hydrogen Energy* **37**, 227 (2012).
17. J.F. Xu, F. Liu, and D. Zhang: In situ observation of solidification of undercooled hypoeutectic Ni–Ni_3B alloy melt. *J. Mater. Res.* **28**, 1891 (2013).
18. J.F. Xu, F. Liu, and B. Dang: Phase selection in undercooled Ni-3.3 Wt Pct B alloy melt. *Metall. Mater. Trans. A* **44**, 1401 (2013).
19. A.M. Mullis, C.R. Clopet, and R.F. Cochrane: Determination of the origin of anomalous eutectic structures from in situ observation of recalescence behaviour. *Mater. Sci. Forum* **790**, 349 (2014).

Supplementary Material

To view supplementary material for this article, please visit http://dx.doi.org/jmr.2015.295.

https://doi.org/10.1557/jmr.2015.295 Published online by Cambridge University Press